CHAPTER 6

Controlling bacterial infection by human dual specificity phosphatase inhibition

Harald M.H.G. Albers, Coenraad Kuijl, Tiziana Scanu, Loes J.D. Hendrickx, Sharida Wekker, Nadha Farhou, Nora Liu, Patrick Celie, Huib Ovaa and Jacques J. Neefjes, *Paper in preparation*.

Abstract. Multidrug resistance (MDR) of bacteria is a serious social threat and a neglected area in the pharmaceutical industry. New intervention strategies besides conventional treatments are required to overcome MDR bacteria. Current treatments use antibiotics that target the pathogen but not the involved host protein pathway required for pathogen survival. Recently, it has been demonstrated by Kuijl *et al.* that H-89 inhibits intracellular growth of *Salmonella (S.) typhimurium* by inhibiting the host's protein kinase PKB/Akt1. Here we describe an RNA interference screen of the human phosphatome that reveals several host dual specificity phosphatases (DUSP3, 11 and 27) that are essential for intracellular growth of *S. typhimurium*. In parallel, screening a tyrosine/dual specificity phosphatase targeted library of small molecules afforded inhibitors that reduced intracellular growth of *S. typhimurium*. One of these identified molecules inhibited the host proteins DUSP3, 11 and 27 confirming the target (DUSPs) lead (inhibitor) relationship for *S. typhimurium* infection. This inhibitor was further developed into a selective inhibitor for DUSP3 (IC_{50} = 0.33 μM) over DUSP27 (IC_{50} > 5 μM) and molecular docking reveals a binding pose of this inhibitor for DUSP3 explaining this selectivity. In conclusion, targeting the host proteins required for pathogen survival appears to be a valid way to control bacterial infection and holds promise as a new therapeutic approach to treat bacterial infections in the clinic.

6.1 Introduction

Bacterial infection is still a big social threat as proven by one of the world's most severe outbreaks of Enterohaemorrhagic *Escherichia coli* (EHEC) in Europe last year.[1] In addition, with multidrug resistance (MDR) of bacteria it becomes increasingly difficult to treat these bacterial infections.[2] New intervention strategies are required next to conventional treatments to overcome MDR in bacteria. Developing medicines that target host proteins essential for bacterial survival instead of killing bacteria directly with antibiotics could be an answer to this problem.

Many bacterial pathogens survive in intracellular compartments of host cells and use that location as a niche for growth while remaining undetected by the immune system.[3] These bacteria frequently remain in such compartments in a dormant state and are therefore difficult to reach by antibodies and antibiotics. For their survival, bacteria need to manipulate the host system to prevent transport from phagosomes to phagolysosomes where they can be degraded.[4,5]

Using a combination of chemistry, small interfering RNA (siRNA) screening, biochemistry and cell biology, we have recently shown that the intracellular bacteria *Salmonella* (*S.*) *typhimurium* activates a signaling network around the protein kinase PKB/Akt1 to prevent delivery to lysosomal compartments where bacteria would otherwise have been degraded (Figure 1A).[5] Bacteria activate the protein kinase PKB/Akt1 for their survival

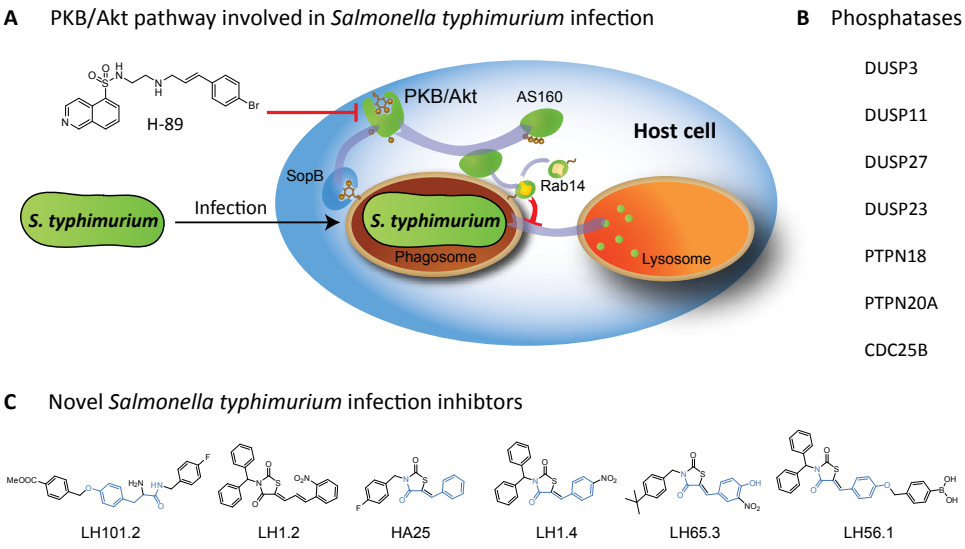

Figure 1: (A) The PKB/Akt1 protein pathway involved in *Salmonella (S.) typhimurium* infection. By inhibiting PKB/Akt1 using small molecule inhibitor H-89, intracellular growth of *S. typhimurium* can be blocked. (B) Identified phosphatases by siRNA screening that reduce intracellular growth of *S. typhimurium* in human cells. (C) Novel identified *S. typhimurium* infection inhibitors by screening a tyrosine-based small molecule library (blue: tyrosine motif).

and we inhibited this protein kinase with a commercial inhibitor (H-89, Figure 1A) which induced the bacterial elimination in human cells.[5]

We now report the identification of protein phosphatases that control intracellular growth of *S. typhimurium* in the human host cell. The function of only few protein phosphatases is known and this class of enzymes is studied relatively poorly compared to protein kinases. Protein phosphatases are divided in three main classes based on their phosphorylated protein substrates; serine/threonine phosphatases, tyrosine phosphatases and dual specificity phosphatases (DUSP).[6] The latter class is able to hydrolyze both phosphorylated serine, threonine and tyrosine residues and is member of the protein tyrosine phosphatase family. By silencing all protein phosphatases (Supporting Table S1) of the human host cell we have mainly identified protein tyrosine phosphatases, which control intracellular bacterial growth of *S. typhimurium* (Figure 1B). Among these identified protein tyrosine phosphatases several DUSPs were present (DUSP3, 11 and 27).

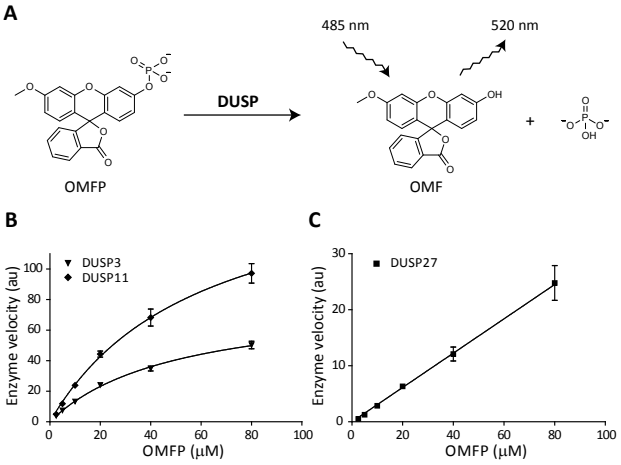

Figure 2: (A) DUSP activity assay using OMFP as substrate. (B) Saturation curves for DUSP3 and 11. (C) Linear relationship of the phosphate hydrolysis velocity of DUSP27 and substrate concentration.

We tested a tyrosine-based small molecule library designed to target protein tyrosine phosphatases, including DUSPs. This library partly consisted of the previously described ATX inhibitors in Chapter 3. Compounds depicted in Figure 1C reduced the intracellular growth of *S. typhimurium* in host cells to a similar extent as obtained through phosphatase silencing. Important to note, these compounds were not toxic for *S. typhimurium* or the host cell alone (see Supporting Figures S1 and S2).

In this study we show that one of the identified inhibitors of intracellular growth of *S. typhimurium* act on the identified host DUSPs. Medicinal chemistry efforts then resulted in a selective DUSP3 inhibitor, which is a challenging task in the development of phosphatase inhibitors. The selectivity of this compound can be explained by molecular docking of this inhibitor into DUSP3 and 27 crystal structures.

6.2 Enzyme kinetics of DUSP3, 11 and 27

In order to test *S. typhimurium* inhibitors on DUSP activity we have developed an activity assay using 3-*O*-methylfluorescein phosphate (OMFP) as DUSP substrate (Figure 2A).[7] The quenched

OMFP substrate is hydrolyzed by the DUSPs into the fluorophore 3-*O*-methylfluorescein (OMF) and phosphate. First we studied the enzyme kinetics of DUSP3, 11 and 27 (Figure 2B and C) using this assay. DUSP3 and 11 show normal Michaelis–Menten kinetics giving saturation at high substrate concentration (Figure 2B) while DUSP27 shows a linear relationship between enzyme velocity and substrate concentration (Figure 2C). The Michaelis constants (K_m values) for DUSP3 and 11 are 50 µM and 59 µM, respectively. Due to the linear kinetics of DUSP27 its K_m is infinite under these conditions.

6.3 Effect of *S. typhimurium* inhibitors on DUSP activity

The compounds that reduced intracellular growth of *S. typhimurium* in human host cells have been tested on their effect on the the activity of the three DUSPs. DUSP activity was measured at an OMFP concentration of 20 µM using an inhibitor concentration of 5 µM (Figure 3). The most active compound that inhibited all the three DUSPs is LH65.3 with high percentage inhibitions (PI) between 85% and 97%. This inhibitor did not show any preference for a specific DUSP (Figure 4A).

6.4 Structure-activity relationships of DUSP inhibitors

In order to increase the potency and selectivity of LH65.3 for the three DUSPs we synthesized analogs of this inhibitor. For this purpose we changed the benzyl (R1) and benzylidene (R2) moieties as depicted in Table 1. Activities of the compounds for DUSP3, 11 and 27 were measured as percentage inhibition (PI) at an inhibitor concentration of 5 µM. First we replaced the 4-*tert*-butyl benzyl (R1) moiety in LH65.3 by 4-nitroacetophenone (**1**), 4-trifluoromethyl benzyl (**2**), diphenyl methane (**3**), 2-(methyl)naphthalene (**4**), 4-bromo benzyl (**5**) and 4-fluoro benzyl (**6**). None of the modifications improved the activity of the inhibitors (Table 1). Next, we changed the position of the nitro and hydroxyl moiety in LH65.3 (compounds **7** and **14**) which had a negative effect on DUSP inhibition. However, introduction of a methoxy group on the *meta* position (**21**) afforded full inhibition for all the three DUSPs. We then explored structure-activity relationships (SAR) of all the possible combinations of the previously described R1 and R2 groups (Table 1). In general, having a 4-hydroxy-3-methoxy-5-nitrophenyl moiety for R1 (**21**-**26**) has a positive effect on the potency of the inhibitors leading to almost full inhibition for the three DUSPs. The nature of the R1 group doesn't seem to have a

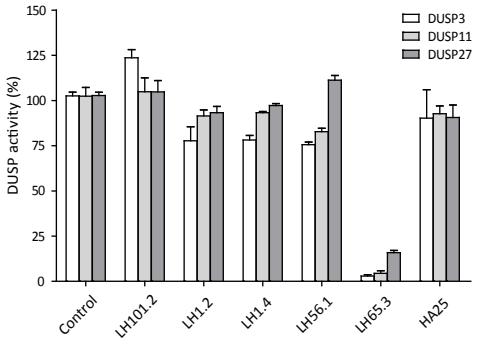

Figure 3: Effect of identified *S. typhimurium* infection inhibitors on the activity of DUSP3, 11 and 27. DUSP activity (%) has been measured at an inhibitor concentration of 5 µM.

Table 1: Structure-activity relationships of DUSP inhibitors. Percentage inhibition (PI, %) at 5 µM of compound are given for DUSP3, 11 and 27, respectively.

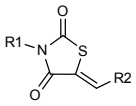

R1 \ R2		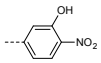		
	LH65.3 97 ± 1 DUSP3 96 ± 1 DUSP11 84 ± 1 DUSP27	**7** 49 ± 3 41 ± 4 22 ± 4	**14** 28 ± 7 26 ± 2 20 ± 4	**21** 98 ± 1 98 ± 1 94 ± 1
	**1** 22 ± 1 14 ± 1 10 ± 3	**8** 98 ± 1 99 ± 1 40 ± 1	**15** 81 ± 6 62 ± 7 22 ± 2	**22** 99 ± 1 99 ± 1 92 ± 1
	**2** 71 ± 12 65 ± 6 53 ± 3	**9** 89 ± 10 80 ± 2 34 ± 3	**16** 43 ± 2 35 ± 6 29 ± 3	**23** 99 ± 1 100 ± 1 99 ± 1
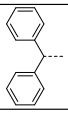	**3** 68 ± 4 66 ± 6 53 ± 2	**10** 70 ± 6 53 ± 5 33 ± 6	**17** 70 ± 7 69 ± 4 56 ± 1	**24** 98 ± 1 99 ± 1 96 ± 1
	**4** 91 ± 1 85 ± 1 68 ± 4	**11** 87 ± 3 64 ± 5 22 ± 3	**18** 66 ± 3 57 ± 8 33 ± 3	**25** 96 ± 2 93 ± 2 84 ± 3
	**5** 96 ± 1 86 ± 8 47 ± 3	**12** 69 ± 3 56 ± 2 25 ± 1	**19** 48 ± 4 49 ± 2 30 ± 2	**26** 96 ± 1 98 ± 1 95 ± 1
	**6** 6 ± 2 6 ± 4 9 ± 1	**13** 42 ± 5 25 ± 1 13 ± 1	**20** 10 ± 1 8 ± 2 7 ± 4	**27** 10 ± 1 12 ± 10 15 ± 1

0-30% 30-60% 60-90% 90-100%

large negative effect on the activity of the compounds when R2 is 4-hydroxy-3-methoxy-5-nitrophenyl, with the only exception when R1 is 4-fluoro benzyl (**27**). Overall, poor activities were obtained for R1 as a 4-fluoro benzyl moiety (**6**, **13**, **20** and **27**), most of the activities (PI) for these compounds were below 15%.

6.5 Selectivity and mode of inhibition of inhibitor 8

For the most active compounds in Table 1 that evidenced full DUSP3 inhibition (dark green boxes) we have determined IC_{50} values for all the three DUSPs (Table 2) in order to find selective DUSP inhibitors. Obtained IC_{50} values for the inhibitors varied between 0.33 and 2.4 µM. We were able to improve the activity of our reference inhibitor,

Table 2: IC_{50} values (µM) for the ten most potent DUSP inhibitors sorted by decreasing potency for DUSP3.

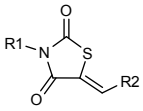

Entry	R1	R2	DUSP3	DUSP11	DUSP27
8	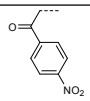		0.33 ± 0.06	0.73 ± 0.06	> 5.00
23		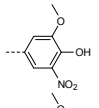	0.59 ± 0.08	0.66 ± 0.03	0.94 ± 0.06
25		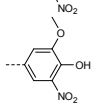	0.93 ± 0.09	1.01 ± 0.09	0.70 ± 0.01
24	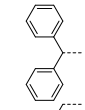		1.21 ± 0.20	1.23 ± 0.02	1.45 ± 0.06
4			1.27 ± 0.25	1.67 ± 0.09	2.53 ± 0.23
21		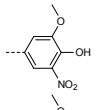	1.36 ± 0.05	1.35 ± 0.08	1.79 ± 0.03
26			1.40 ± 0.02	1.35 ± 0.07	1.65 ± 0.02
LH65.3			1.53 ± 0.05	1.57 ± 0.06	1.86 ± 0.05
5			1.62 ± 0.08	2.11 ± 0.10	1.81 ± 0.04
22			1.74 ± 0.27	2.11 ± 0.17	2.43 ± 0.03

LH65.3, by a 5 fold for DUSP3 resulting in inhibitor **8**. More importantly, inhibitor **8** is selective for DUSP3 (IC_{50} = 0.33 µM) compared to DUSP11 and 27 (IC_{50} = 0.73 µM and IC_{50} > 5 µM). In Figure 4A and 4B the dose-response curves for LH65.3 and **8** are depicted to visualize the gain in potency and selectivity of **8** for the three DUSPs compared to LH65.3.

Next, we studied the mode of inhibition of **8** using Lineweaver-Burk analysis. For DUSP3 and 11, inhibitor **8** showed non-competitive inhibition (Figure 4C). Increasing the inhibitor concentration of inhibitor **8** did not change the V_{max} or K_m of DUSP27 (Figure 4C).

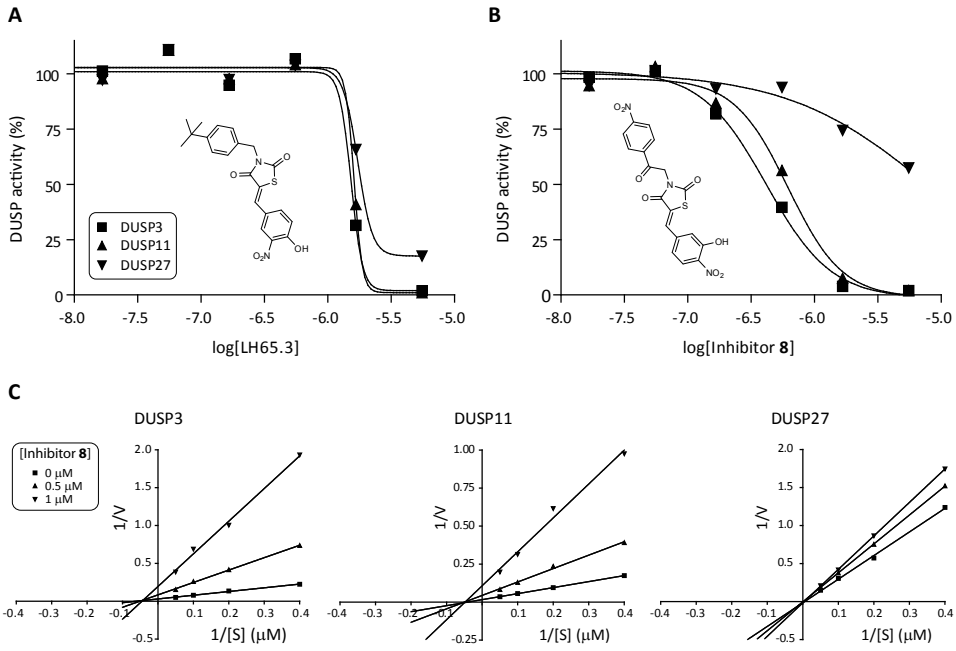

Figure 4: Selectivity and mode of inhibition. (A) Dose response curves for LH65.3. (B) Dose response curves for inhibitor **8**. (C) Lineweaver-Burk analysis of inhibitor **8** for DUSP3, 11 and 27.

6.6 Protein surface comparison between DUSP3 and 27

In order to explain the selectivity of inhibitor **8** for DUSP3 over DUSP27 we compared the protein surfaces of these two DUSPs. Several crystal structures of DUSP3 have been reported[8-10] but not for DUSP27 at the time of this study. Therefore we crystallized DUSP27 to make a structural comparison with DUSP3 (for details concerning the crystallization see Experimental section). In Figure 5 the electrostatic surfaces of DUSP3,[10] inactive DUSP3 (C124S mutant) bound to a phosphorylated p38 peptide,[8] and DUSP27 are displayed. In DUSP3 two pockets are clearly visible, the catalytic pocket (P1) and an arginine pocket (P2). The phosphorylated p38 peptide binds to these pockets with its phosphorylated tyrosine residue and phosphorylated serine residue to P1 and P2, respectively.[8] The P1 and P2 pocket in DUSP3 are separated by a cleft were the p38 peptide still can bind. In DUSP27 this catalytic pocket P1 is clearly visible but the P2 pocket is not as abundantly present as in DUSP3. A clear difference between DUSP3 and 27 can be observed in the electrostatic surface potential. DUSP3 and inactive DUSP3 have identical electrostatic surfaces while DUSP27 is displaying a reversed electrostatic surface compared to DUSP3. This reversed electrostatic surface between DUSP3 and 27 has been predicted using an DUSP27 homology model[11] and confirmed by a recently resolved DUSP27 structure[12] and our data.

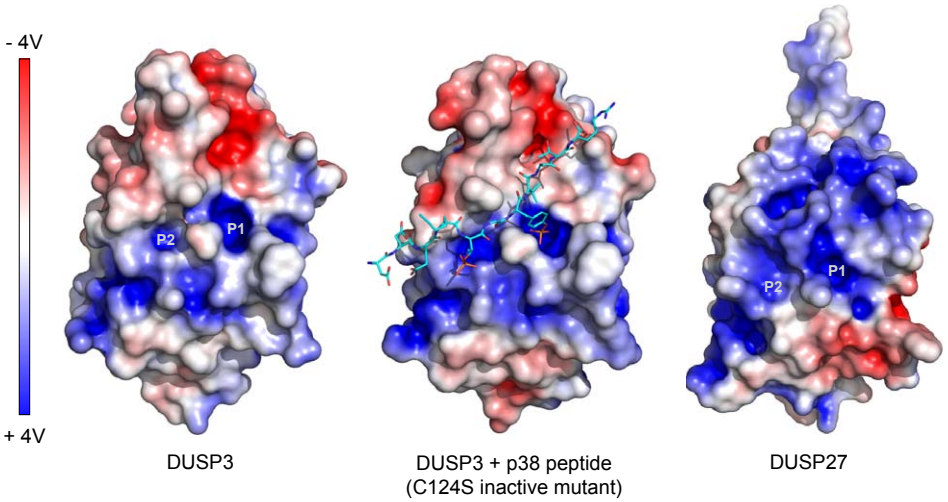

Figure 5: Surface representation displaying the electrostatic surface (blue is positive, red is negative) of the crystal structures of DUSP3 (PDB ID: 1VHR), inactive DUSP3 (C124S mutant) binding to a phosphorylated p38 peptide (PDB ID: 1J4X) and DUSP27. Catalytic site is indicated with P1 and an arginine pocket with P2.

6.7 Molecular docking of inhibitor 8 with DUSP3 and 27

Intrigued by the differences in the surfaces of DUSP3 and 27 we reasoned that molecular docking of inhibitor **8** with these two DUSPs could explain why this inhibitor is selective for DUSP3 over DUSP27. In our docking approach, using the program Autodock, we used a large docking site around catalytic pocket P1 and arginine pocket P2 (docking space, 30 Å x 30 Å x 30 Å) to see whether inhibitor **8** has a preference for a different binding site than P1 and P2. However, the best binding site of inhibitor **8** for DUSP3 and 27 was catalytic pocket P1 (Figure 6). The best docking pose of inhibitor **8** for DUSP3

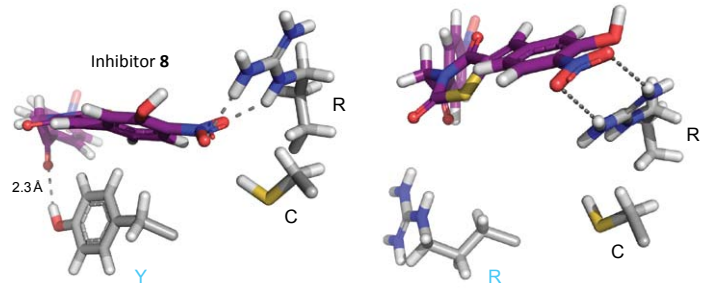

Protein:	**DUSP3**	**DUSP27**
Catalytic sequence:	HCREGYSR	HCVMGRSR
Docking energy:	- 8.0 kcal mol^{-1}	- 6.4 kcal mol^{-1}

Figure 6: Molecular docking suggests that inhibitor **8** (deep purple) binds in proximity of catalytic arginine residue (R) of DUSP3 and 27. A hydrogen bond is observed between a tyrosine residue (Y) in the DUSP3 active site with the indicated carbonyl of inhibitor **8**, this interaction is not possible in DUSP27.

revealed an interaction with the catalytic arginine residue R130 of DUSP3 with the nitro group in **8**. In addition, there is a hydrogen bond between the carbonyl of the 4-nitroacetophenone moiety in **8** with tyrosine residue Y128 (Figure 6). This hydrogen bond is not observed for the best docking pose of inhibitor **8** in DUSP27 because the tyrosine residue in not conserved in DUSP27 and is replaced by an arginine residue (Figure 6). This hydrogen bond of **8** with DUSP3 is a logical explanation why the affinity of **8** for DUSP3 (IC_{50} = 0.33 µM) is much higher than for DUSP27 (IC_{50} > 5 µM) and also for the higher predicted binding energy of inhibitor **8** for DUSP3 (-8.0 kcal mol^{-1} versus -6.4 kcal mol^{-1}).

6.8 Conclusions and Discussion

This study shows that the host proteins DUSP3, 11 and 27 of the host cell are essential for intracellular growth of the bacteria *S. typhimurium*. In our approach we used a small interfering RNA (siRNA) screen of the human phosphatome and a reversed chemical screen. In the latter methodology we screened tyrosine-based small molecules as a general tyrosine/ dual specificity phosphatase inhibitor library. One of the molecules (LH65.3) that resulted from the small molecule screen inhibited the identified DUSPs 3, 11 and 27 confirming the phosphatase target-inhibitor relationship.

Further development of LH65.3 resulted in a selective DUSP3 inhibitor (**8**) which has poor affinity for DUSP27. Molecular docking suggests that a hydrogen bond exists between inhibitor **8** and tyrosine residue Y130 in DUSP3 which is not present in DUSP27. This hydrogen bond probably explains the higher affinity of this inhibitor for DUSP3 over DUSP27.

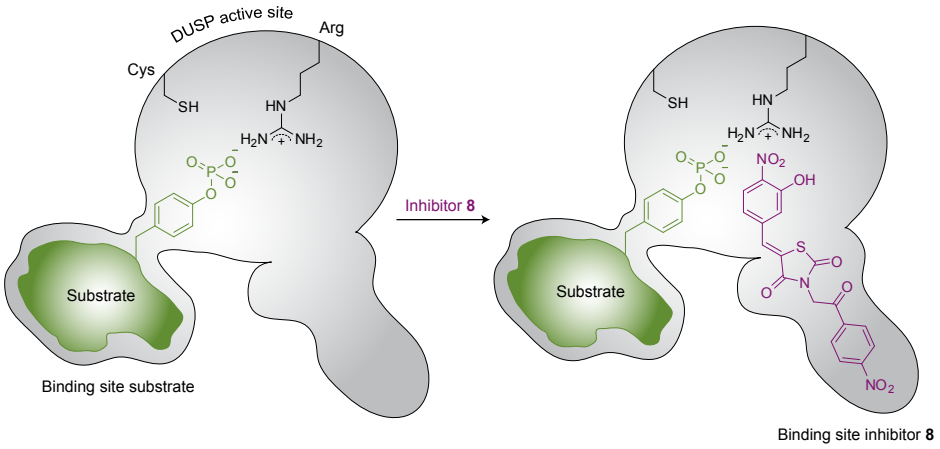

Figure 7: Model proposing the binding of inhibitors and tyrosine phosphorylated substrate with DUSP family phosphatases. Here DUSP inhibitor **8** (purple) is depicted as example. Tyrosine moieties of a substrate (green) and inhibitor **8** are located in the active site while the remaining part of these molecules binds to a different site in DUSP. Only the catalytic residues cysteine and arginine are depicted for clarity.

Development of selective phosphatase inhibitors is a challenging task because of their close homology.

Somewhat controversial is the fact that the mode of inhibition for this selective inhibitor **8** is non-competitive. The tyrosine moiety in this inhibitor is introduced to target the phosphatase active site. In addition, unbiased molecular docking of inhibitor **8** shows a preference for the catalytic site of DUSP3 and 27. Our hypothesis explaining our results is depicted in Figure 7. In this model the binding site of tyrosine moieties of a tyrosine phosphorylated DUSP substrate and selective inhibitor **8** are in proximity of each other in the large DUSP active site while the remaining parts of the molecules bind to different sites outside the DUSP active site. A crystal structure of inhibitor **8** in complex with DUSP3 or 27 should reveal its true binding.

In conclusion, targeting host DUSP proteins essential for bacterial growth seems to be a valid way to fight bacterial infection and holds promise as a new therapeutic strategy to treat these infections. This new approach could be a useful addition to the current bacterial infection treatments that target solely the bacteria itself.

6.9 Experimental section

General. See Experimental section Chapter 4.

Synthesis inhibitor library. Inhibitors were synthesized as previously described with minor adjustments to the protocol.[13-15] In short, to a cooled solution (277 K) of thiazolidine-2,4-dione (5.87 g, 50 mmol) in DMF (100 ml) sodium hydride (60% in oil, 1.8 g, 45 mmol) was added. A solution of the appropriate benzyl bromide (36.8 mmol) in DMF (25 ml) was added to the reaction mixture. The mixture was allowed to warm up to room temperature and was stirred for 4 h. Then the mixture was poured into of ice water (250 ml) and hexane (100 ml) was added. After a night at 277 K the precipitated crystals were filtrated and dried to give *N*-alkylated thiazolidine-2,4-dione.

The resulting *N*-alkylated thiazolidine-2,4-dione (0.317 mmol) was dissolved in ethanol (2.5 mL) containing piperidine (70 μL, 0.709 mmol) and the appropriate aldehyde (0.348 mmol) was added and the solution was refluxed overnight. Upon cooling to room temperature the product precipitated out of solution. Centrifugation and washing with ethanol gave homogeneous compound.

(*Z*)-3-(4-(tert-butyl)benzyl)-5-(4-hydroxy-3-nitrobenzylidene)thiazolidine-2,4-dione (LH65.3). Yield: 20%. **^{1}H NMR:** δ = 8.20 (d, *J* = 2.3, 1H), 7.95 (s, 1H), 7.77 (dd, *J* = 2.3, 8.8, 1H), 7.37 (d, *J* = 8.5, 2H), 7.25 (dd, *J* = 8.6, 11.0, 3H), 4.79 (s, 2H), 1.25 (s, 9H). **^{13}C NMR:** δ = 166.93, 165.37, 153.69, 150.28, 137.43, 135.51, 132.46, 131.63, 127.80, 127.49, 125.40, 123.93, 120.15, 119.96, 44.38, 34.21, 31.02. **MS:** m/z $[M+H]^+$ calc. 413.12, obs. 412.92.

(*Z*)-5-(3-hydroxy-4-nitrobenzylidene)-3-(2-(4-nitrophenyl)-2-oxoethyl)thiazolidine-2,4-dione (8). Yield: 26%. **^{1}H NMR:** δ = 8.41 (d, *J* = 9.0, 2H), 8.33 (d, *J* = 9.1, 2H), 8.02 (d, *J* = 8.5, 1H), 7.99 (s, 1H), 7.39 (d, *J* = 1.7, 1H), 7.27 (dd, *J* = 1.6, 8.6, 1H), 5.45 (s, 2H). **^{13}C NMR:** δ = 190.94, 166.52, 164.77, 152.44, 150.61, 138.63, 138.23, 137.53, 131.84, 129.89, 126.13, 124.36, 124.00, 120.47, 119.81, 48.28. **MS:** m/z $[M+H]^+$ calc. 430.03, obs. 429.87.

Phosphatase siRNA screen. Gene silencing was performed in 96 well plates with a human breast cancer (MCF-7) and glioblastoma (A-172) cell line. Cells were seeded at a density of 5000 cells per well and reverse transfected with DharmaFECT transfection reagent #4 and 50 nM siRNA (Human siGenome SMARTpool phosphatase library, Dharmacon). Two days after transfection, cells were infected with *S. Typhimurium* expressing DsRed[16] was performed based on the infection protocol described by Steele-Mortimer *et al*. with minor changes.[17] In short, two days before infection a bacterial culture was streaked from the frozen stock on LB agar plate. The next day, an overnight bacterial culture was prepared by inoculating 5 mL LB medium with one colony from the agar plate. The overnight culture was incubated at 310 K and 200 rpm for 16-20 h and then diluted 1:33 in fresh, pre-warmed (310 K) ampicillin (100 μg mL^{-1}) containing LB medium for a further incubation of 3.5 h. The bacterial culture (4 mL) was transferred to a 15 ml Falcon tube and pelleted in 4000 rpm for 10 min at room temperature. The pellet was washed once with DMEM/FCS and resuspended in DMEM/FCS full medium (310 K). The cells were infected with an MOI of 50 for 20 min. After infection the cells were washed 4 times with DMEM/FCS containing 100 μg mL^{-1} gentamycin and remaining extracellular bacteria were killed by addition of DMEM/FCS medium with 100 μg mL^{-1} gentamicin for 60 min. For the remaining infection period, the antibiotic concentration was lowered to 10 μg mL^{-1}. After overnight infection cells were washed once with PBS and 30 μL of trypsin/EDTA was added for 5 min followed by addition of 30 μL PBS/BSA 1%. The sample was fixed by addition of 60 μL PBS formalin 7%.

Samples were analyzed by flow cytometry (BD FACSArray) for DsRed fluorescence as marker for Salmonella infection and proliferation. The data were normalized (cellHTS2, Bioconductor) and transformed into Z-scores.[18]

Small molecule screen. The infection of mammalian cells (MCF-7 or A172) with *S. typhimurium* expressing DsRed[16] was performed based on the infection protocol described by Steele-Mortimer *et al*. with minor changes.[17] In short, two days before infection a bacterial culture was streaked from the frozen stock on an ampicillin containing LB agar plate. The next day, an overnight bacterial culture was prepared by inoculating 5 mL of ampicillin containing LB medium with one colony from the agar plate. The overnight culture was incubated at 310 K and 200 rpm for 16-20 h and then diluted 1:33 in 5 mL fresh, pre-warmed (310 K) ampicillin containing LB medium for a further incubation of 3.5 h. 4 mL the culture was transferred to 15 mL Falcon tube and pelleted at 4000 rpm for 10 min at room temperature. The pellet was washed once with DMEM/FCS and resuspended in DMEM/FCS (310 K). In order to infect the cells with the MOI 20 for 30 min, the bacterial culture was diluted according to the following assumption: OD_{595} of 1 ≈ 1.3 x 10^9 CFU mL^{-1}. To infect cells with bacteria, the cell culture medium was aspirated and 100 μL of bacteria in DMEM/FCS was added to the wells. Plates were centrifuged at 1000 rpm at room temperature for 5 min and incubated at 310 K with 5% CO_2 in a humidified cell culture incubator to allow invasion for 1 h. The cells were washed 4 times with DMEM/FCS containing 100 μg mL^{-1} gentamycin and incubated for another 1 h in DMEM/FSC containing 100 μg mL^{-1} gentamycin. For the remaining infection period, the media was replaced with DMEM/FCS containing 10 μg mL^{-1} gentamicin and compound if indicated. Compounds were tested at 10 μM in triplicate.

After overnight infection cells were washed once with PBS and incubated in 30 μl of trypsin/EDTA for 5-10 min. Subsequently, 30 μL PBS/1% BSA was added used to resuspend the cells. 60 μL PBS/formalin (7%) was added to fix cells and bacteria. After at least 2 h samples were measured by FACS as previously described.

Effect of compounds on *S. typhimurium* growth in LB medium. An overnight bacterial culture was prepared by inoculating 5 mL of ampicillin (100 μg mL^{-1}) containing LB medium with one colony

from an agar plate. The overnight culture was incubated at 310 K and 200 rpm for 16-20 h and then diluted 1:33 in fresh ampicillin (100 μg mL^{-1}) containing LB medium. In a 96-wells plate, 100 μL of the bacteria containing medium was pipetted to an LB medium (100 μL) containing 20 μM of inhibitor. Bacterial growth was monitored by measuring the optical density at 595 nm (OD_{595}).

Cell toxicity. See Experimental section Chapter 2.

DUSP activity assay.[7] Measuring DUSP activity using 3-*O*-methylfluorescein phosphate (OMFP) as a substrate[19] was determined as follows. In a black flat-bottom 96-wells plate was added 0.9 μL DMSO containing inhibitor, to 45 μL recombinant DUSP (~0.1 U) in a Tris-HCl buffer (9 mM Tris-HCl, 11 mM NaCl, 1 mM EDTA, 1 mM DTT, 0.01% triton X-100, pH 7.4). Finally, 45 μL of 40 μM OMFP in the previously described Tris-HCl buffer was added to each well using a multichannel pipet and instantaneously fluorescence was measured at room temperature ($\lambda_{ex}/\lambda_{em}$ = 485/520 nm). The above described mixture with DMSO alone was used as a positive control. OMFP without DUSP was taken as control for auto-hydrolysis of OMFP. For each inhibitor percentage inhibition (PI) was determined at a final inhibitor concentration of 5 μM. IC_{50} values of inhibitors have been determined in an inhibitor concentration range of 0.01 to 6 μM. Data were analyzed using Graphpad Prism software. In addition, the effect of the inhibitors on the fluorescence of the produced OMF was investigated using ~1 μM OMF at an inhibitor concentration of 5 μM (Supporting Figure S3).

Cloning, expression and purification of DUSPs. PCR fragments of phosphatase domains of DUSP3, 11 and 27 (Supporting Table S2) containing a His-tag sequence have been cloned into a pETNKI-His-3c-LIC-kan vector[20] and were sequence verified. The resulting constructs have been transformed into BL21 (DE3) cells. Transformed cells were grown overnight in LB medium (2 mL) containing kanamycin (30 μg mL^{-1}) and were subsequently inoculated in LB medium (1 L) with kanamycin (30 μg mL^{-1}) until an OD_{595} of 0.6 was reached. Protein expression was induced by IPTG (0.5 mM) overnight at 293 K. Cells were spun down (3,000 x g, 15 min, 277 K) and the resulting cell pellet was resuspended in a Tris buffer (40 mM Tris, 200 mM NaCl, 5 mM β-mercaptoethanol, 5 mM imidazol, pH 8.0). After sonification the resuspension the cell debris and insoluble proteins were removed by centrifugation (14,000 x g, 30 min, 277 K) and the soluble fraction was incubated with Talon beads and washed with the above described Tris buffer. The Talon beads were eluted with a Tris buffer (40 mM Tris, 200 mM NaCl, 5 mM β-mercaptoethanol, 300 mM imidazol, pH 8.0) and collected fractions were analyzed on an SDS-PAGE gel. Fractions containing solely DUSP protein were pooled and purified by resource Q anion-exchange chromatography. For crystallization purpose, the His-tag purification label of DUSP27 was removed by GST-tagged 3C protease cleavage overnight at 277 K. A final purification step of all DUSPs involved a S75 gel filtration using as eluent a Tris buffer (40 mM Tris, 100 mM NaCl, 5 mM β-mercaptoethanol, pH 8.0) resulting in a pure protein solution which was concentrated using a Centriprep column.

DUSP27 Crystallization. Screening of crystallization conditions for DUSP27 was performed at nanoliter scale in 96-well format. 200 nL sitting drops (100 nL DUSP27 (5 mg mL^{-1}) and 100 nL reservoir solution) were prepared by the Mosquito dispensing robot (TTP Labtech) using the PACT and JCSG+ screens.[21] Crystallization plates were stored and imaged at 277 K by the RockImager (Formulatrix) and at 293 K by the CrystalFarm (Bruker-AXS). Initial microcrystals and needle-like crystals were observed at 277 K in conditions from the PACT screen containing 0.1 M bis-Tris propane (pH 6.5 and pH 7.5), 20% PEG 3350 and either 0.2 M sodium nitrate, 0.2 M sodium fluoride or 0.2 M sodium-potasium phosphate. These crystals were used in microseeding experiments against the PACT and JCSG+ screen. Briefly, crystals were transferred to 75 μL of reservoir solution in an eppendorf

tube and vortexed for 30 s. Sitting drops were prepared from 100 nL of DUSP27 (5 mg mL^{-1}), 100 nL reservoir solution and 10 nL seed solution. Crystals were observed in multiple conditions and further optimization of these conditions was performed using the Formulator microfluidics liquid dispensing robot (Formulatrix) with microseeding. Suitable crystals for X-ray diffraction studies were obtained at 277 K in 0.1 M Tris pH 8.0, 21% PEG 3350, 0.2 M sodium sulphate; in 0.1 M Tris pH 7.2, 12% PEG 8000; in 0.1 M Tris pH 7.5, 0.2 M magnesium chloride and 16% PEG 6000. Crystals appeared as needles and as plates, with typical dimensions of 0.05 x 0.1 x 0.3 mm and 0.1 mm x 0.2 mm x 0.25 mm, respectively.

Data collection and structure refinement. DUSP27 X-ray diffraction data was collected at 100 K from a crystal grown in 0.1 M Tris pH 7.5, 0.2 M magnesium chloride and 16% PEG 6000 at our home source (Microstar Ultra II (Bruker-AXS) with Mar345 image plate detector (Marresearch)). The crystal was cryoprotected in 0.1 M Tris pH 7.5, 0.2 M magnesium chloride, 18% PEG 6000 and 20% glycerol before freezing in liquid nitrogen solution. 100 images were collected with 1 degree oscillation and 120 s exposure per frame and a crystal to detector distance of 200 mm (2.21 Å resolution at the edge of the detector). The diffraction data set was indexed and integrated using Mosflm[22] and scaled using SCALA.[23] Molecular replacement using the structure of DUSP13 (PDB ID: 2PQ5) as search model, was performed in Phaser.[24] An initial model was build and revealed 2 molecules in the asymmetric unit. The model was subjected to automated tracing in ARP/wARP[25] and was further refined using the software programs Refmac in CCP4[26] interspersed with manual rebuilding in Coot.[27] Data collection and refinement statistics can be found in Supporting Table S3.

Molecular docking, protein and ligand preparation. The X-ray structures of DUSP3 (PDB ID: 1VHR) and DUSP27 were used for docking studies. The protein and ligand structures were prepared using Autodock version 1.5.4. The initial 3D structures of the ligands were generated using CORINA. We defined a region for docking by a 30 Å x 30 Å x 30 Å box centered around the P1 and P2 pocket of DUSP3 and 27. Final docking experiments were done using Autodock Vina.[28] Graphics were made using PyMOL 1.3.

6.10 References

1. Turner, M. Microbe outbreak panics Europe. *Nature (London, U. K.)* **474**, 137 (2011).
2. Nikaido, H. Multidrug resistance in bacteria. *Annu. Rev. Biochem.* **78**, 119-146 (2009).
3. Vergne, I. Chua, J. Singh, S. & Deretic, V. Cell Biology of Mycobacterium Tuberculosis Phagosome. *Annu. Rev. Cell Dev. Biol.* **20**, 367-394 (2004).
4. Uchiya, K. & Nikai, T. Salmonella enterica Serovar Typhimurium Infection Induces Cyclooxygenase 2 Expression in Macrophages: Involvement of Salmonella Pathogenicity Island 2. *Infect. Immun.* **72**, 6860-6869 (2004).
5. Kuijl, C. et al. Intracellular bacterial growth is controlled by a kinase network around PKB/AKT1. *Nature* **450**, 725-730 (2007).
6. Hunter, T. Protein kinases and phosphatases: The Yin and Yang of protein phosphorylation and signaling. *Cell* **80**, 225-236 (1995).
7. Tierno, M. et al. Development and optimization of high-throughput in vitro protein phosphatase screening assays. *Nat. Protoc.* **2**, 1134-1144 (2007).
8. Schumacher, M. Todd, J. Rice, A. Tanner, K. & Denu, J. Structural Basis for the Recognition of a

Bisphosphorylated MAP Kinase Peptide by Human VHR Protein Phosphatase. *Biochemistry* **41**, 3009-3017 (2002).

9. Wu, S. et al. Multidentate Small-Molecule Inhibitors of Vaccinia H1-Related (VHR) Phosphatase Decrease Proliferation of Cervix Cancer Cells. *J. Med. Chem.* **52**, 6716-6723 (2009).
10. Yuvaniyama, J. Denu, J. Dixon, J. & Saper, M. Crystal Structure of the Dual Specificity Protein Phosphatase VHR. *Science* **272**, 1328-1331 (1996).
11. Friedberg, I. et al. Identification and characterization of DUSP27, a novel dual-specific protein phosphatase. *FEBS Lett.* **581**, 2527-2533 (2007).
12. Lountos, G. Tropea, J. & Waugh, D. Structure of human dual-specificity phosphatase 27 at 2.38Å resolution. *Acta Cryst. D* **67**, 471-479 (2011).
13. Albers, H. M. et al. Discovery and Optimization of Boronic Acid Based Inhibitors of Autotaxin. *J. Med. Chem.* **53**, 4958-4967 (2010).
14. Albers, H. M. et al. Structure-Based Design of Novel Boronic Acid-Based Inhibitors of Autotaxin. *J. Med. Chem.* **54**, 4619-4626 (2011).
15. Albers, H. M. et al. Boronic acid-based inhibitor of autotaxin reveals rapid turnover of LPA in the circulation. *Proc. Natl. Acad. Sci. USA* **107**, 7257-7262 (2010).
16. Sörensen, M. et al. Rapidly maturing red fluorescent protein variants with strongly enhanced brightness in bacteria. *FEBS Lett.* **552**, 110-114 (2003).
17. Steele-Mortimer, O. Méresse, S. Gorvel, J. Toh, B. & Finlay, B. B. Biogenesis of Salmonella typhimurium-containing vacuoles in epithelial cells involves interactions with the early endocytic pathway. *Cell. Microbiol.* **1**, 33-49 (1999).
18. Boutros, M. Bras, L. & Huber, W. Analysis of cell-based RNAi screens. *Genome Biol.* **7**, R66 (2006).
19. Tamura, K. et al. Cdc25 Inhibition and Cell Cycle Arrest by a Synthetic Thioalkyl Vitamin K Analogue. *Cancer Res.* **60**, 1317-1325 (2000).
20. Luna-Vargas, M. et al. Enabling high-throughput ligation-independent cloning and protein expression for the family of ubiquitin specific proteases. *J. Struct. Biol.* **175**, 113-119 (2011).
21. Egan, D. et al. Towards rationalization of crystallization screening for small- to medium-sized academic laboratories: the PACT/JCSG+ strategy. *Acta Cryst. D* **61**, 1426-1431 (2005).
22. Leslie, A. G. W. Recent changes to the MOSFLM package for processing film and image plate data. *Joint CCP4 + ESF-EAMCB Newsletter on Protein Crystallography* **26**, (1992).
23. Evans, P. Scaling and assessment of data quality. *Acta Cryst. D* **62**, 72-82 (2006).
24. McCoy, A. et al. Phaser crystallographic software. *J. Appl. Cryst.* **40**, 658-674 (2007).
25. Perrakis, A. Morris, R. & Lamzin, V. Automated protein model building combined with iterative structure refinement. *Nat. Struct. Mol. Biol.* **6**, 458-463 (1999).
26. Collaborative Computational Project, N. The CCP4 suite: programs for protein crystallography. *Acta Cryst. D* **50**, 760-763 (1994).
27. Emsley, P. Lohkamp, B. Scott, W. G. & Cowtan, K. Features and development of Coot. *Acta Cryst. D* **66**, 486-501 (2010).
28. Trott, O. & Olson, A. AutoDock Vina: Improving the speed and accuracy of docking with a new scoring function, efficient optimization, and multithreading. *J. Comput. Chem.* **31**, 455-461 (2010).

6.11 Supporting information

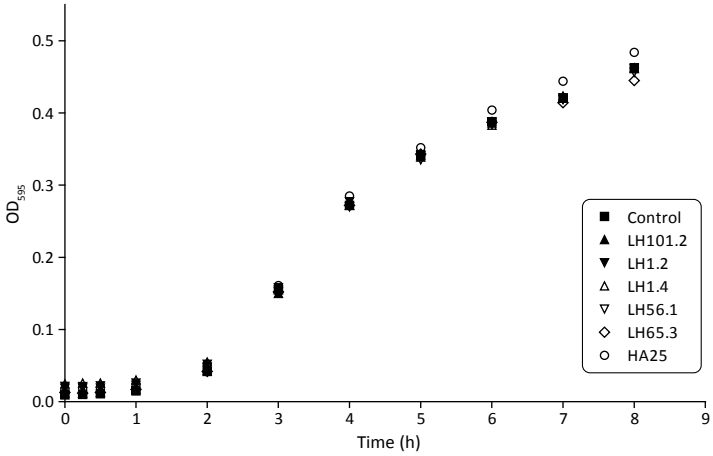

Supporting Figure S1: Effect of compounds on *S. typhimurium* growth in LB medium. Bacterial growth of *S. typhimurium* was measured in the presence or absence of 10 µM of compound at a wavelength of 595 nm. Data points have not been fitted for clarity.

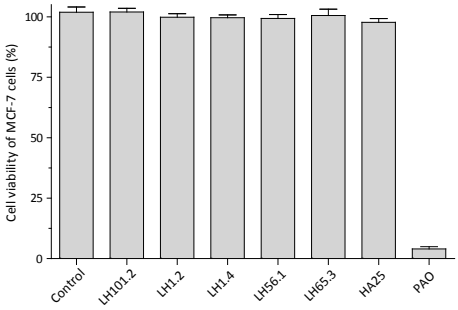

Supporting Figure S2: Effect of compounds on cell viability of MCF-7 cells. Cell viability of MCF-7 cells was tested using the conditions of the *S. typhimurium* FACS assay. Compounds were incubated for 42 h at a concentration of 10 µM. Phenylarsine oxide (PAO) was used as a control for cell death.

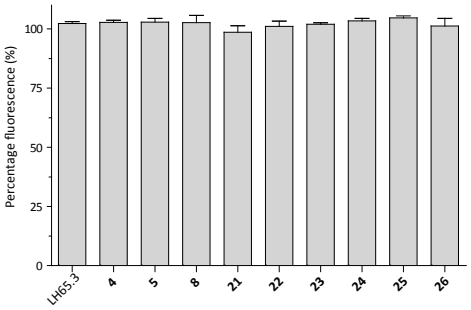

Supporting Figure S3: Effect of DUSP inhibitors on DUSP activity assay readout. Fluorescence of OMF was measured at an inhibitor concentration of 5 µM.

Supporting Table S1: List of screened phosphatase and phosphatase-like siRNAs

Name	Catalog number	Locus id	Accession id	Name	Catalog number	Locus id	Accession id
ENPP2	M-004601-01	5168	NM_006209	DUSP13	M-007887-00	51207	NM_016364
PTPN6	M-009778-00	5777	NM_002831	DUSP14	M-007888-00	11072	NM_007026
C7ORF16	M-018324-01	10842	NM_006658	DUSP15	M-008484-01	128853	NM_080611
CDKN3	M-003879-00	1033	NM_005192	DUSP18	M-007891-00	150290	NM_152511
DUSP1	M-003484-02	1843	NM_004417	DUSP19	M-007892-01	142679	NM_080876
DUSP10	M-003965-01	11221	NM_007207	DUSP21	M-007893-01	63904	NM_022076
DUSP2	M-003565-01	1844	NM_004418	DUSP23	M-007909-00	54935	NM_017823
DUSP22	M-004517-00	56940	NM_020185	MGC1136	M-008027-01	78986	NM_024025
DUSP4	M-003963-02	1846	NM_001394	MGC26484	M-008030-00	168448	XM_171149
DUSP5	M-003566-01	1847	NM_004419	MK-STYX	M-008031-01	51657	NM_016086
DUSP6	M-003964-01	1848	NM_001946	MTMR1	M-008037-01	8776	NM_003828
DUSP7	M-003567-00	1849	XM_037430	MTMR2	M-008038-00	8898	NM_016156
DUSP8	M-003568-00	1850	NM_004420	MTMR4	M-008040-01	9110	NM_004687
ILKAP	M-010260-00	80895	NM_030768	MTMR7	M-008041-00	9108	XM_044727
PFKFB1	M-006761-00	5207	NM_002625	PDP2	M-022572-00	57546	NM_020786
PFKFB2	M-006762-01	5208	NM_006212	PPEF1	M-009479-00	5475	NM_006240
PFKFB3	M-006763-00	5209	NM_004566	PPEF2	M-012250-01	5470	NM_006239
PFKFB4	M-006764-00	5210	NM_004567	PPM1B	M-008281-01	5495	NM_002706
PPP1R1B	M-012745-00	84152	NM_032192	PPM1E	M-008964-00	22843	NM_014906
PPP2CA	M-003598-00	5515	NM_002715	PPM1F	M-009544-00	9647	NM_014634
PPP4C	M-008486-01	5531	NM_002720	PPM1G	M-005264-01	5496	NM_002707
PTPN5	M-003600-01	84867	NM_032781	PPM1L	M-008679-00	151742	NM_139245
PTPRG	M-008069-00	5793	NM_002841	PPM2C	M-008718-00	54704	NM_018444
PTPRJ	M-008476-01	5795	NM_002843	PPP1CA	M-008927-00	5499	NM_002708
PTPRR	M-004017-01	5801	NM_002849	PPP1CB	M-008685-00	5500	NM_002709
PTPRT	M-008072-01	11122	NM_007050	PPP2R1A	M-010259-01	5518	NM_014225
TRIO	M-005047-00	7204	NM_007118	PPP2R5A	M-009352-01	5525	NM_006243
ACYP2	M-008864-00	98	NM_138448	PPP2R5B	M-009366-00	5526	NM_006244
PPP1R16B	M-004065-00	26051	NM_015568	PPP2R5C	M-009433-00	5527	NM_002719
PPP2R3A	M-017376-00	5523	NM_002718	PPP2R5D	M-009799-01	5528	NM_006245
SAG	M-011105-00	6295	NM_000541	PPP2R5E	M-008531-01	5529	NM_006246
ZFHX1B	M-006914-00	9839	NM_014795	PPP3CC	M-010005-00	5533	NM_005605
ACP5	M-009615-01	54	NM_001611	PPP5C	M-009259-00	5536	NM_006247
PPP3CA	M-008300-01	5530	NM_000944	PPP6C	M-009935-01	5537	NM_002721
PSPH	M-011888-01	5723	NM_004577	PTP4A1	M-006333-01	7803	NM_003463
ACP1	M-019058-00	52	NM_004300	PTP4A2	M-009078-00	8073	NM_003479
ACPP	M-009262-00	55	NM_001099	PTP4A3	M-006859-01	11156	NM_007079
CDC14A	M-003469-00	8556	NM_003672	PTPDC1	M-008584-00	138639	NM_152422
CDC14B	M-003470-02	8555	NM_003671	PTPLA	M-008742-00	9200	NM_014241
CDC25A	M-003226-02	993	NM_001789	PTPN1	M-003529-04	5770	NM_002827
CDC25B	M-003227-02	994	NM_004358	PTPN11	M-003947-01	5781	NM_002834
CDC25C	M-003228-01	995	NM_001790	PTPN12	M-008064-01	5782	NM_002835
DUSP11	M-007885-00	8446	NM_003584	PTPN13	M-008065-00	5783	NM_006264
EPM2A	M-006896-01	7957	NM_005670	PTPN21	M-009379-01	11099	NM_007039
PPAP2B	M-017312-01	8613	NM_003713	PTPN22	M-008066-00	26191	NM_012411
PPAP2C	M-011500-00	8612	NM_003712	PTPN23	M-009417-00	25930	NM_015466
PPM1D	M-004554-00	8493	NM_003620	PTPN3	M-009372-01	5774	NM_002829
PPP1R3C	M-017077-00	5507	NM_005398	PTPN4	M-009489-01	5775	NM_002830
PTEN	M-003023-01	5728	NM_000314	PTPN7	M-008394-00	5778	NM_002832
PTPN14	M-008509-00	5784	NM_005401	PTPN9	M-008832-00	5780	NM_002833
PTPRU	M-009328-01	10076	NM_005704	PTPRA	M-004519-00	5786	NM_002836
TPTE2	M-008107-00	93492	NM_130785	PTPRB	M-004994-02	5787	NM_002837
CTDP1	M-009326-01	9150	NM_004715	PTPRC	M-008067-00	5788	NM_002838
DUSP12	M-007886-01	11266	NM_007240	PTPRD	M-008527-00	5789	NM_002839

Name	Catalog number	Locus id	Accession id
PTPRE	M-008068-02	5791	NM_006504
PTPRF	M-008375-01	5792	NM_002840
PTPRH	M-009448-00	5794	NM_002842
PTPRK	M-004204-01	5796	NM_002844
PTPRM	M-006326-00	5797	NM_002845
PTPRN	M-009315-01	5798	NM_002846
PTPRN2	M-008070-00	5799	NM_002847
ACP2	M-008205-00	53	NM_001610
INPP5B	M-021811-01	3633	NM_005540
ALPPL2	M-003455-01	251	NM_031313
PPP3R1	M-009869-01	5534	NM_000945
IGBP1	M-011298-01	3476	NM_001551
ANP32E	M-015844-00	81611	NM_030920
LPPR4	M-009911-00	9890	NM_014839
PPP2CB	M-003599-02	5516	NM_004156
ENPP1	M-003809-01	5167	NM_006208
MAP3K7IP1	M-004770-00	10454	NM_006116
ACP6	M-008665-00	51205	NM_016361
INPP5D	M-003013-01	3635	NM_005541
DUT	M-010258-00	1854	NM_001948
SYNJ1	M-019486-01	8867	NM_003895
PPP1R11	M-011917-01	6992	NM_021959
DKFZP761G058	M-018772-00	152926	NM_152542
FLJ40125	M-009006-00	147699	NM_178494
AKAP11	M-009277-01	11215	NM_016248
BPNT1	M-008664-01	10380	NM_006085
PPM1A	M-009574-01	5494	NM_021003
ACPT	M-008366-01	93650	NM_033068
PHPT1	M-016904-00	29085	NM_014172
ENPP3	M-004540-00	5169	NM_005021
PTPN2	M-008969-00	5771	NM_002828
PPP1R7	M-019589-00	5510	NM_002712
LOC151242	M-023104-00	151242	XM_087137
HSPC129	M-008272-00	51496	NM_016396
MTM1	M-008036-01	4534	NM_000252
ALPP	M-003454-01	250	NM_001632
MTMR3	M-008039-01	8897	NM_021090
ENPP4	M-009214-01	22875	NM_014936
PON1	M-009229-00	5444	NM_000446
IMPA1	M-010172-01	3612	NM_005536
PPP1R8	M-010903-00	5511	NM_002713
PPP2R4	M-005214-00	5524	NM_021131

Name	Catalog number	Locus id	Accession id
C21ORF6	M-013856-00	10069	NM_016940
DUSP3	M-007894-00	1845	NM_004090
ALPI	M-008673-00	248	NM_001631
TPTE	M-008745-01	7179	NM_013315
ENPP5	M-009805-01	59084	NM_021572
PON2	M-009676-00	5445	NM_000305
IMPA2	M-008348-00	3613	NM_014214
PPP2R2A	M-004824-01	5520	NM_002717
OCRL	M-010026-01	4952	NM_000276
ENPP7	M-009059-00	339221	NM_178543
PTPRS	M-009662-01	5802	NM_002850
SSH3	M-008937-00	54961	NM_017857
FBP2	M-010139-01	8789	NM_003837
PPAP2A	M-019098-00	8611	NM_003711
INPP1	M-008505-01	3628	NM_002194
PR48	M-019459-00	28227	NM_013239
PIB5PA	M-009108-00	27124	NM_014422
TENS1	M-009997-00	64759	NM_022748
C14ORF24	M-018433-00	283635	NM_173607
STYX	M-009571-01	6815	NM_145251
PTPN18	M-009385-00	26469	NM_014369
RNGTT	M-009782-00	8732	NM_003800
FHIT	M-004952-01	2272	NM_002012
SYNJ2	M-012624-00	8871	NM_003898
PPP1CC	M-006827-00	5501	NM_002710
PME-1	M-005211-00	51400	NM_016147
CILP	M-008295-00	8483	NM_003613
FLJ23751	M-008557-00	92370	NM_152282
FRMPD2	M-008854-00	143162	NM_152428
MINPP1	M-009705-00	9562	NM_004897
PTPRZ1	M-009685-00	5803	NM_002851
INPP4B	M-011539-00	8821	NM_003866
ALPL	M-008658-00	249	NM_000478
PPP1R2	M-015361-00	5504	NM_006241
I-4	M-012962-00	80316	NM_025210
RWDD2	M-015117-00	112611	NM_033411
DNAJC6	M-009885-00	9829	NM_014787
ENPP6	M-008704-00	133121	NM_153343
FBP1	M-008725-00	2203	NM_000507
PPP2R2B	M-003022-01	5521	NM_004576
PTPRO	M-008500-01	5800	NM_002848

Supporting Table S2: Amino acid sequences of DUSP3, 11 and 27. The catalytic domain containing the HCXXGXXR motif is underlined.

DUSP	Amino acid sequence
3	MAHHHHHHSAALEVLFQGPGMSGSFELSVQDLNDLLSDGSGCYSLPSQPCNEVTPRIYVGN ASVAQDIPKLQKLGITHVLNAAEGRSFMHVNTNANFYKDSGITYLGIKANDTQEFNLSAYF ERAADFIDQALAQKNGRVLVHCREGYSRSPTLVIAYLMMRQKMDVKSALSIVRQNREIGPN DGFLAQLCQLNDRLAKEGKLKP
11	MAHHHHHHSAALEVLFQGPGRFIAFKVPLQKSFEKKLAPEECFSPLDLFNKIREQNEELGL IIDLTYTQRYYKPEDLPETVPYLKIFTVGHQVPDDETIFKFKHAVNGFLKENKDNDKLIGV HCTHGLNRTGYLICIYLIDVEGVRPDDAIELFNRCRGHCLERQNYIEDLQNGPIRKNWNSS VPRSSDFEDSAHLMQPVHNKPVKQGPRYNLHQIQGHSAPRHFHTQTQSLQQSVRKFSENPH VY
27 [a]	**MAHHHHHHSAALEVLFQG**PGYTHVNEVWPKLYIGDEATALDRYRLQKAGFTHVLNAAHGRW NVDTGPDYYRDMDIQYHGVEADDLPTFDLSVFFYPAAAFIDRALSDDHSKILVHCVMGRSR SATLVLAYLMIHKDMTLVDAIQQVAKNRCVLPNRGFLKQLRELDKQLVQQRRRSQRQDGEE EDGREL

[a] *In bold the amino acid sequence removed by GST-tagged 3C protease for crystallization purposes.*

Supporting Table S3: Data collection and refinement statistics for DUSP27.

	DUSP27
Data collection	
Space group	$P2_12_12$
Cell dimensions	
a, *b*, *c* (Å)	56.11, 60.62, 54.55
a, b, g (°)	90, 90, 90
Resolution (Å)	2.2 (2.33-2.2)
R_{sym} or R_{merge}	0.094 (0.54)
I / s*I*	4.0 (3.4)
Completeness (%)	97.6 (97.6)
Redundancy	3.8 (3.6)
Refinement	
Resolution (Å)	20-2.2
No. reflections	8598
R_{work} / R_{free}	0.28/0.32
R.m.s. deviations	
Bond lengths (Å)	0.012
Bond angles (°)	1.508

APPENDICES

Summary and future prospects

Nederlandse samenvatting

Curriculum Vitae

List of publications

Nawoord